

# Boosting ZnO nanowire dye-sensitized solar cell efficiency by coating a porous ZnO layer on the nanowires

Yufu Zhu · Fei Deng · Chaoying Ni ·  
Wenzhong Shen

Received: 3 June 2014 / Accepted: 22 July 2014 / Published online: 8 August 2014  
© Springer Science+Business Media New York 2014

**Abstract** Novel ZnO core/shell nanostructures were constructed by depositing a porous ZnO layer directly on the surfaces of pre-fabricated ZnO nanowires through a facile chemical method. The morphology and structure of the obtained products have been investigated by field-emission scanning electron microscopy, high-resolution transmission electron microscopy and X-ray diffraction analysis. In these unique nanostructures, the porous overlayer exhibits a large surface area for sufficient dye loading to enhance light harvesting and the ZnO nanowire cores provide direct conduction pathways for the photogenerated electron transport to diminish the chance of electron recombination. The obtained ZnO nanostructures were used as photoanode material in dye-sensitized solar cell which showed an increase in performance of 141 % compared with an equivalent solar cell employing ZnO nanowire arrays as photoanode. This result was achieved mainly due to an increase in photogenerated current density directly resulting from improved light harvesting of the porous layer.

## 1 Introduction

In the past two decades, dye-sensitized solar cells (DSCs) have attracted considerable attention due to their advantages of cost-effectiveness, ease of fabrication and environmental friendliness [1–10]. In order to fabricate DSCs with high performance, a large surface area and fast electron transport of the photoanode material is required. It is widely accepted that the performance of DSC is closely related to the morphologies of the photoanode films. Therefore, rational synthesis of nanostructures with unique morphologies would be very important for DSC applications.

Up to now, metal oxide nanostructures, especially TiO<sub>2</sub> and ZnO, have been widely used in DSCs [4–10]. Compared with TiO<sub>2</sub>, ZnO has higher electron mobility [8]. The high mobility of ZnO should result in a rapid electron transfer and a reduced probability of electron recombination. Therefore, the application of ZnO nanowires in DSCs is of great interest. However, reported efficiencies of ZnO nanowire solar cells are very low at present [5, 11–14]. One possible reason for the low efficiency may be that the surface area of the nanowire photoanode is not large enough. As we all know, photoanode films with porous frameworks have also been widely used in DSCs due to their large specific surface area [4, 15, 16]. Although the porous film can provide a large specific surface area, the photogenerated electrons will interact with a lot of traps when they transport in the porous film. In order to keep the merits and avoid the demerits of the photoanode films at the same time, we were motivated to develop a novel core/shell structural film with ZnO nanowires as cores and a porous ZnO overlayer as shells. The porous ZnO shells exhibit a large surface area for dye loading and the ZnO nanowire cores provide direct conduction pathways for the

---

Y. Zhu (✉)  
Jiangsu Provincial Key Laboratory for Interventional Medical  
Devices, Huaiyin Institute of Technology, Huaian 223003, China  
e-mail: zhuyufu@yahoo.com

Y. Zhu · F. Deng · C. Ni  
Department of Materials Science and Engineering, University of  
Delaware, Newark, DE 19716, USA

W. Shen  
Institute of Solar Energy, and Key Laboratory of Artificial  
Structures and Quantum Control (Ministry of Education),  
Department of Physics and Astronomy, Shanghai Jiao Tong  
University, Shanghai 200240, China

**Table 1** Preparation conditions for photoanode Nos. 1–3 (HMT and PEI are the abbreviation for “hexamethylenetetramine” and “polyethyleneimine”, respectively)

Photoanodes	Substrates	Zinc nitrate (mM)	Zinc acetate (mM)	HMT (mM)	PEI (mM)	Ammonium hydroxide (mL)	Solvent	Temperature (°C)
No. 1	FTO with ZnO seeds	25	0	25	5	1.2	Pure water	88
No. 2	Photoanode No. 1	0	60	30	0	0	1 mL deionized water and 49 mL methanol	62
No. 3	Photoanode No. 1	0	60	30	0	0	4 mL deionized water and 46 mL methanol	62

photogenerated electron transport. Therefore, the overall efficiency of DSC based on the unique nanostructures is expected to be increased and it is quite necessary to synthesize the unique nanostructures for DSC application.

In this paper, a two-step chemical method was developed for the synthesis of novel nanostructures composed of ZnO nanowire cores and porous ZnO shells. In step-one, highly-ordered ZnO nanowire arrays were deposited on FTO (fluorine doped tin oxide, SnO<sub>2</sub>:F) substrates. In step-two, porous ZnO was synthesized on the surfaces of the step-one prepared nanowires. It was found that the composition of the solvent used in step-two played an important role in determining the final product morphology. The obtained nanostructures were successfully used as photoanode material in DSCs and it was revealed that the DSC based on ZnO nanowires with porous surfaces showed an increase in performance of 141 % compared with an equivalent solar cell employing ZnO nanowire arrays with smooth surface.

## 2 Experimental details

### 2.1 Synthesis of ZnO nanostructures and fabrication of DSCs

Details of the process for the synthesis of ZnO nanowire arrays on FTO substrates can be found in Table 1 (Photoanode No. 1) and Ref. [17]. The FTO substrates with ZnO nanowire arrays grown on them were then transferred into a glass bottle consisting 60 mM anhydrous zinc acetate [Zn(CH<sub>3</sub>COO)<sub>2</sub>] and 30 mM hexamethylenetetramine (HMT). The solution used here was prepared with a mixed solvent of methanol and water. The covered bottle was then heated at 62 °C for 15 h. The detailed preparation conditions were shown in Table 1 (Photoanode Nos. 2 and 3). After deposition, the yielded product was finally washed, dried, and calcinated at 500 °C for 60 min. The obtained ZnO nanostructures were all sensitized in a 0.5 mM of the N719 dye and used as photoanode in DSCs. An FTO substrate with a layer of sputtered Pt film was used as

counter-electrode. The liquid electrolyte used in the DSCs was a 0.6 M tetra-butylammonium iodide, 0.1 M iodine, 0.1 M lithium iodide, and 0.5 M 4-tert-butylpyridine in acetonitrile.

### 2.2 Characterizations

The morphology and structure of products were characterized by field-emission scanning electron microscope (FESEM; JEOL JSM-7400F), high-resolution transmission electron microscope (HRTEM; JEOL JEM-2010F) and X-ray diffraction (XRD; Rigaku D-Max) analysis. The photocurrent-photovoltage characteristics of the fabricated DSCs were measured by means of a computer-controlled Keithley 2400 source-meter under an oriel solar simulator (100 mW/cm<sup>2</sup>).

## 3 Results and discussion

### 3.1 Morphology and structure of the obtained ZnO nanorod arrays

Figure 1a shows cross-sectional SEM image of the yielded ZnO nanowire arrays. It is obvious that high density arrays of ZnO nanowires have been synthesized on the FTO substrate. The length of the ZnO nanowires is about 11 μm. From the top-view SEM image of the obtained ZnO nanowire arrays shown in Fig. 1b, one can easily find out that the diameters of the nanowires are not uniform. The XRD pattern of the product is demonstrated in Fig. 1c. Except for those coming from the FTO substrate, all the diffraction peaks can be well indexed as the wurtzite phase ZnO [Joint Committee for Powder Diffraction Standards (JCPDS) no. 36–1451]. It is noted that the intensity of the XRD pattern has been normalized to facilitate comparisons. The measured intensities of other peaks were normalized to that of the (002) peak. From Fig. 1c, one can easily obtain that the (002) peak is very strong, which is due to the preferred orientation of the ZnO nanowire arrays, as displayed in Fig. 1a.

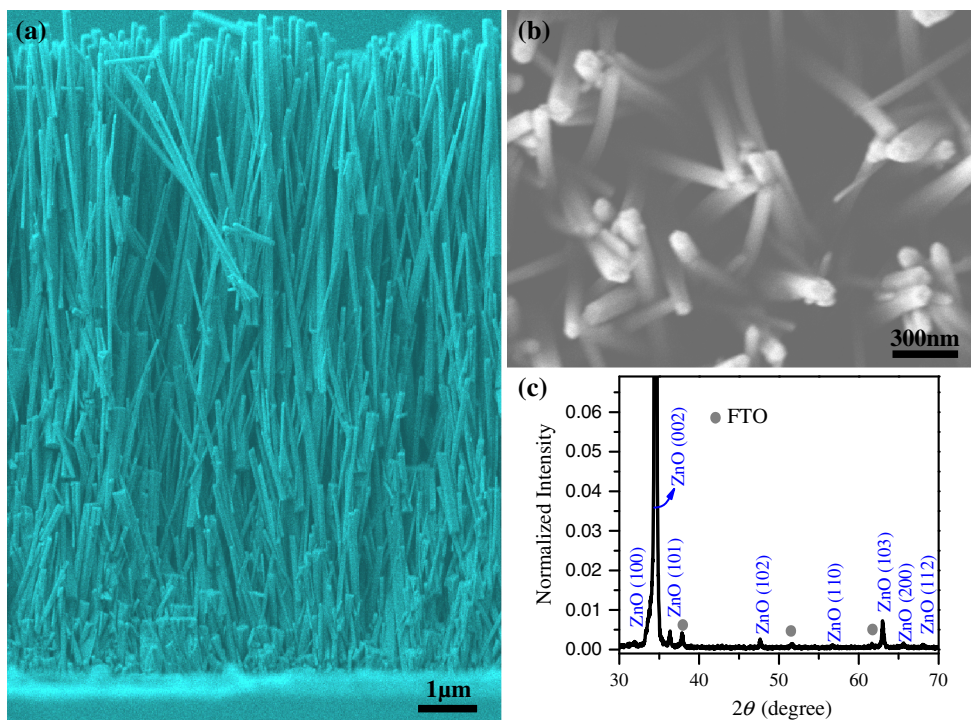


**Fig. 1** **a** Cross-sectional SEM image, **b** top-view SEM image, and **c** XRD pattern of the synthesized ZnO nanowire arrays. This sample is denoted as photoanode No. 1

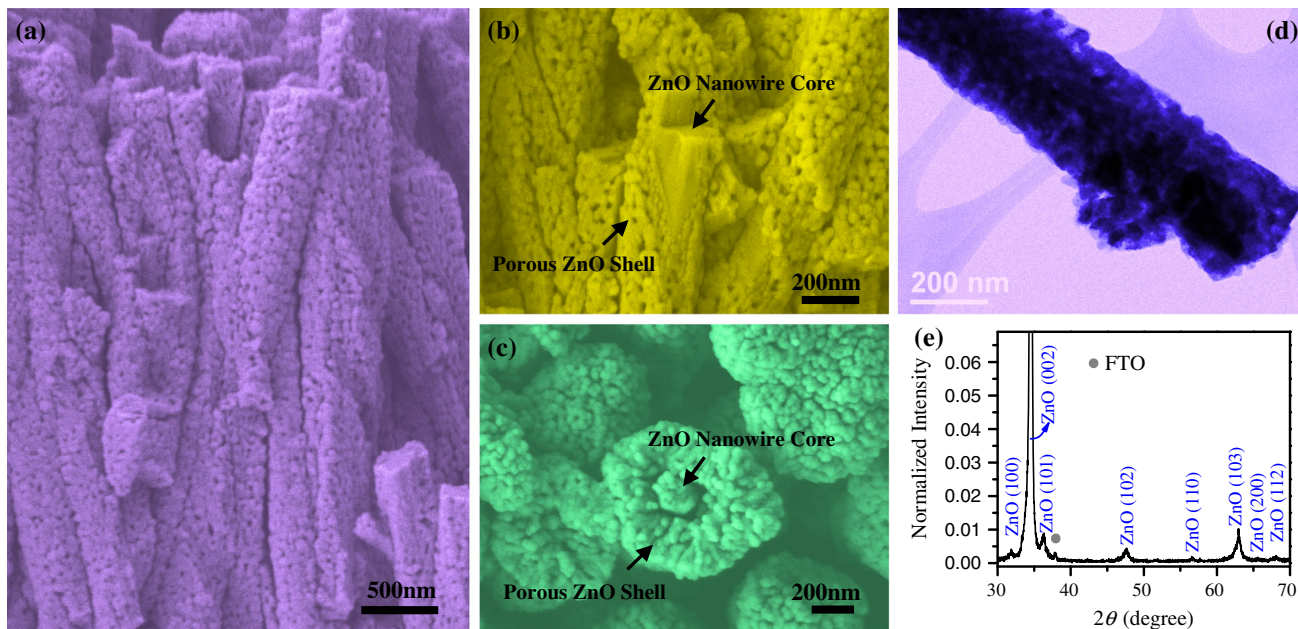


**Fig. 2** **a** Cross-sectional SEM image of ZnO nanowire arrays with porous surfaces, **b** and **c** SEM images of the broken nanowires, **d** TEM image and **e** XRD pattern of the obtained product. This sample is denoted as photoanode No. 2

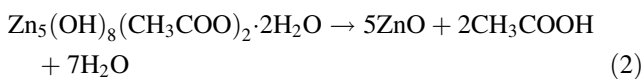
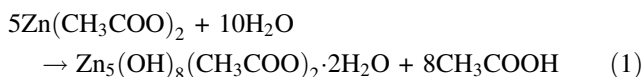
### 3.2 Morphology and structure of the obtained ZnO nanorod arrays with porous surfaces

As demonstrated in both Fig. 1a, b, the surfaces of the nanowires are very smooth. The smooth surface of the obtained

nanowire array is disadvantageous for dye loading and light harvesting. In order to increase the surface area of the photoanode film, the above synthesized nanowire arrays were used as substrates for coating a layer of porous structures. The cross-sectional SEM image of the final product was displayed

in Fig. 2a. From which one can see that the porous nanostructure uniformly cover the surfaces of the step-one prepared nanowires. The broken nanowires presented in Fig. 2b, c clearly demonstrate that the prepared nanostructures are composed of ZnO nanowire cores and porous shells forming the core/shell structures. The corresponding TEM image depicted in Fig. 2d also indicates the porous surface structure of the yielded product. The XRD pattern of the core/shell nanostructures demonstrated in Fig. 2e is very similar to that of the ZnO nanowire arrays shown in Fig. 1c. No other impurity diffraction peaks were detected, indicating the porous layer has the same structure as the ZnO nanowire array.

During the porous layer formation process, we believe the following chemical reactions are involved.



The evidence for the above chemical reactions can be found in the previously reported work [18]. According to the time-dependent experiment results described in Ref. [18],  $\text{Zn}_5(\text{OH})_8(\text{CH}_3\text{COO})_2 \cdot 2\text{H}_2\text{O}$  was formed in the early stage [Eq. (1)] and the synthesis of ZnO was finally realized, as shown in Eq. (2). During the experimental process, the addition of HMT in the chemical solution will accelerate the chemical reactions described in Eqs. (1) and (2) by slowly releasing  $\text{OH}^-$  ions. The corresponding chemical reactions can be described as follows:



Because of the additional  $\text{OH}^-$  ions as expressed in Eq. (4), the addition of HMT in the solution will promote the nucleation and coarsening of ZnO, forming the porous layer on the nanowire surface. However, it is worth noting that the concentration of ZnO formed in the solution should not be too high because the quantity of deionized water added in the methanolic solution also controls the reaction velocity, as described in Eq. (1). The solvent used for the synthesis of porous shell (Fig. 2a) is composed of 1 mL deionized water and 49 mL methanol.

The critical role of water was further investigated by performing reactions with different concentrations of water. To demonstrate the importance of water for the synthesis of porous shell, a chemical solution without water was also used during the experimental process. It was found that a methanolic solution of  $\text{Zn}(\text{CH}_3\text{COO})_2$  and HMT did not lead to the formation of any solid phases on the surfaces of nanowires.

A solution with a high concentration of water (4 mL deionized water and 46 mL methanol) was also used to fabricate nanostructures with the other conditions kept the same. Figure 3a shows the oblique-view SEM image of the final products. It is clear that there are a lot of nanoparticles and microspheres deposited on the top of the nanowire arrays. To display the nanostructures clearly, the top-view SEM image of the yielded products is displayed in Fig. 3b. Figure 3c demonstrates the high-magnification SEM image of the area indicated by the rectangle in Fig. 3a. It is obvious that the surfaces of nanowires are also covered by porous nanostructures and those porous nanostructures are jointed together.

As mentioned above, the quantity of deionized water added in the methanolic solution controls the reaction velocity. Because 4 mL of deionized water was added in the growth solution, the formation of the  $\text{Zn}_5(\text{OH})_8(\text{CH}_3\text{COO})_2 \cdot 2\text{H}_2\text{O}$  would develop faster, as expressed in Eq. (1). The formed  $\text{Zn}_5(\text{OH})_8(\text{CH}_3\text{COO})_2 \cdot 2\text{H}_2\text{O}$  will fill the space among the nanowires and deposit on the top of the nanowire arrays. With the reaction time increasing, ZnO phases will be obtained [Eq. (2)]. After ZnO building blocks coalesced via the oriented attachment mechanism, the formation of porous layer on the surfaces of nanowires and the synthesis of microspheres on the top of the nanowire array will be realized. From Figs. 2a and 3a, it can be concluded that the concentration of water in the growth solution plays an important role in determining the morphologies of the final products.

A typical XRD pattern of the yielded product is shown in Fig. 3d. Compared with the XRD result shown in Fig. 1c, one can see that in addition to the strong (002) peak, the other diffraction peaks corresponding to the wurtzite phase ZnO become strong, which should be originated from the newly deposited ZnO nanostructures on nanowire arrays.

The synthesized ZnO nanostructures were all employed to fabricate DSCs. The photocurrent density (J)–voltage (V) characteristics and the corresponding physical values of the DSCs are respectively displayed in Fig. 4 and Table 2. It is clear that after coating a porous layer on ZnO nanowire arrays (Fig. 2a), the short-circuit current density of DSC increases from 4.27 to 7.0 mA/cm<sup>2</sup>. The increment in the short-circuit current density is mainly due to the fact that the surface area of the ZnO nanowire photoanode is increased after a layer of porous shell formed on nanowire surfaces. The large surface area increases dye loading and light harvesting. On the other hand, the nanowire cores provide direct conduction pathways for the photogenerated electron transport, leading to the suppressed electron recombination. Therefore, the obtained novel nanostructures are advantageous for DSC application.

**Fig. 3** **a** An oblique-view SEM image and **b** top-view SEM image of the obtained product, **c** high-magnification SEM image of the area indicated by the rectangle in **a**; **d** XRD pattern of the synthesized nanostructures. This sample is denoted as photoanode No. 3

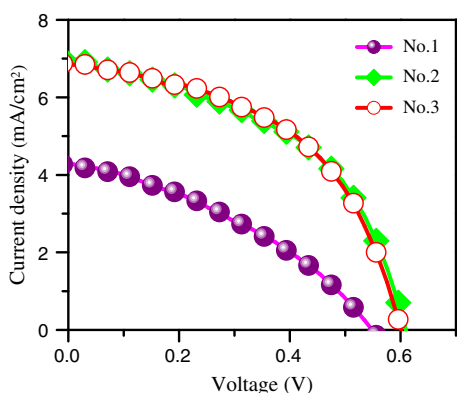
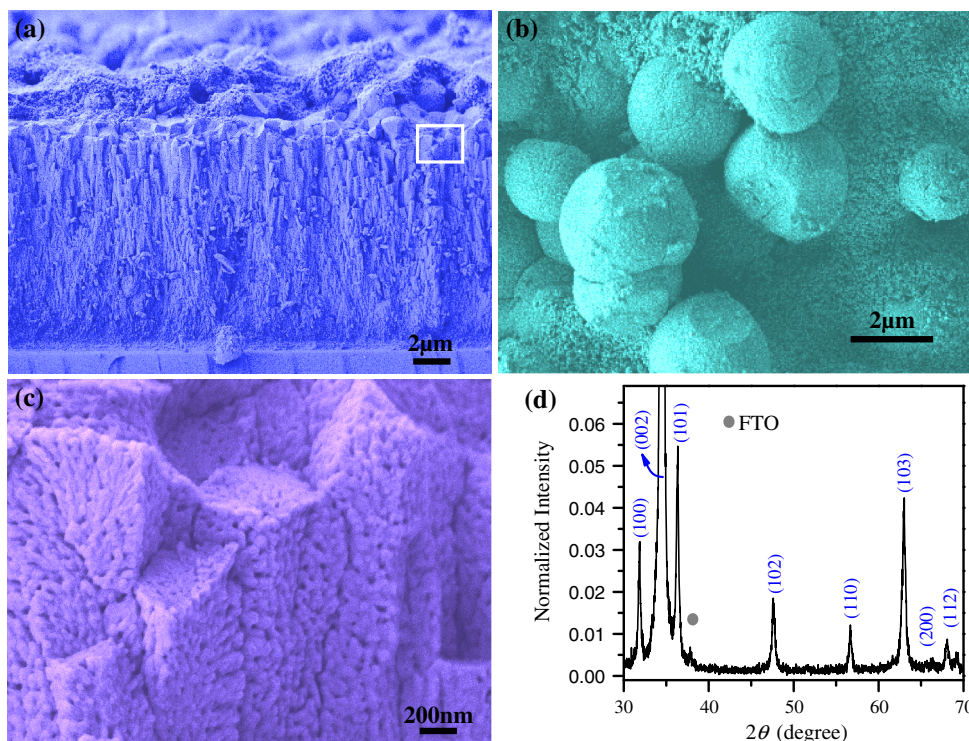


**Fig. 4** Photocurrent-photovoltage characteristics of DSCs based on the fabricated nanostructures

Additional nanoparticles and microspheres deposited on the top of the nanowire arrays (Fig. 3a) should increase the surface area of the photoanode. However, the short-circuit current density of DSC based on photoanode No.3 is

6.85 mA/cm<sup>2</sup>, which shows a small decrease compared with photoanode No. 2. This may be due to the fact that the porous nanostructures are jointed together (Fig. 3c), which is disadvantageous for dye loading. Therefore, the concentration of water in the growth solution plays a pivotal role in determining the morphologies of the photoanodes and the performances of the resulting DSCs.

### 4 Conclusions

In summary, a novel ZnO core/shell nanostructure was successfully synthesized via a facile chemical method. A 141 % increase in energy conversion efficiency was achieved compared with ZnO nanowire array DSC. Although the current work focuses on controllable synthesis and application of the obtained nanostructure in DSCs, the yielded nanostructures are also expected to be used in gas sensors and photocatalysis for improved performance where a large surface area is required.

**Table 2** Photovoltaic parameters of the DSCs using the obtained ZnO nanostructures as photoanodes ( $J_{SC}$ ,  $V_{OC}$  and  $\eta$  are the abbreviation for “short circuit current”, “open circuit voltage” and “light to electricity conversion efficiency”, respectively)

Photoanode	The morphologies of the Photoanodes	$J_{SC}$ (mA·cm <sup>-2</sup> )	$V_{OC}$ (mV)	Fill factor	$\eta$ (%)
No. 1	Fig. 1 (a, b)	4.27	0.55	0.36	0.85
No. 2	Fig. 2 (a–c)	7.00	0.61	0.48	2.05
No. 3	Fig. 3 (a–c)	6.85	0.60	0.50	2.06

**Acknowledgments** This work was supported by the Natural Science Foundation of Jiangsu Province (BK2012244), the National Natural Science Foundation of China (51202081), the National Major Basic Research Project (2012CB934302) and the College Natural Science Foundation of Jiangsu Province (12KJB430003).

## References

1. M. Thambidurai, N. Muthukumarasamy, D. Velauthapillai, C. Lee, *J. Mater. Sci.: Mater. Electron.* **24**, 1921 (2013)
2. P. Jayabal, V. Sasirekha, J. Mayandi, K. Jeganathan, V. Ramakrishnan, *J. Alloys Compd.* **586**, 456 (2014)
3. M. Dadkhah, M. Salavati-Niasari, *Mater. Sci. Semicond. Process.* **20**, 41 (2014)
4. I.Y. Bu, M.T. Cole, *Mater. Lett.* **90**, 56 (2013)
5. T. Ganesh, S.S. Bhande, R.S. Mane, S.H. Han, *Scripta Mater.* **69**, 291 (2013)
6. S. He, X. Zou, Z. Sun, G. Teng, *Mater. Lett.* **91**, 258 (2013)
7. R.T. Ginting, C.C. Yap, M. Yahaya, M. Mat, Salleh, *J. Alloys Compd.* **585**, 696 (2014)
8. I.Y. Bu, *Mater. Sci. Semicond. Process.* **16**, 1730 (2013)
9. E. Tsuji, N. Hirata, Y. Aoki, H. Habazaki, *Mater. Lett.* **91**, 39 (2013)
10. M. Thambidurai, N. Muthukumarasamy, D. Velauthapillai, C. Lee, *J. Mater. Sci.: Mater. Electron.* **24**, 2367 (2013)
11. S. Zhu, X. Chen, F. Zuo, M. Jiang, Z. Zhou, D. Hui, *J. Solid State Chem.* **197**, 69 (2012)
12. A. Tubtimtae, M.W. Lee, *Superlattices Microstruct.* **52**, 987 (2012)
13. S. Vanalakar, S. Mali, R. Pawar, D. Dalavi, A. Mohalkar, H. Deshamukh, P. Patil, *Ceram. Int.* **38**, 6461 (2012)
14. S. Zhu, X. Tian, L. Shan, Z. Ding, Z. Kan, X. Xu, Z. Zhou, L. Wang, *Ceram. Int.* **39**, 9637 (2013)
15. A. Al-Kahlout, *Thin Solid Films* **520**, 1814 (2012)
16. P. Teesetsopon, S. Kumar, J. Dutta, *Int. J. Electrochem. Sci.* **7**, 4988 (2012)
17. C. Xu, P. Shin, L. Cao, D. Gao, *J. Phys. Chem. C* **114**, 125 (2009)
18. H. Wang, C. Xie, D. Zeng, Z. Yang, *J. Colloid Interface Sci.* **297**, 570 (2006)